

Magnetic Nanoparticle-Mediated Targeting of Cell Therapy Reduces In-Stent Stenosis in Injured Arteries

Boris Polyak,^{*,†,§,‡} Mikhail Medved,^{†,‡} Nina Lazareva,[†] Lindsay Steele,^{†,⊥} Tirth Patel,[†] Ahmad Rai,[†] Menahem Y. Rotenberg,^{||} Kimberly Wasko,[†] Andrew R. Kohut,[∇] Richard Sensenig,[#] and Gary Friedman^{†,¶}

[†]Department of Surgery, Drexel University College of Medicine, Philadelphia, Pennsylvania 19102, United States

[§]Department of Pharmacology and Physiology, Drexel University College of Medicine, Philadelphia, Pennsylvania 19102, United States

[⊥]Molecular Cell Biology and Genetics (MCBG) Program, Drexel University College of Medicine, Philadelphia, Pennsylvania 19102, United States

^{||}The Avram and Stella Goldstein-Goren Department of Biotechnology Engineering, Ben-Gurion University of the Negev, Beer-Sheva 84105, Israel

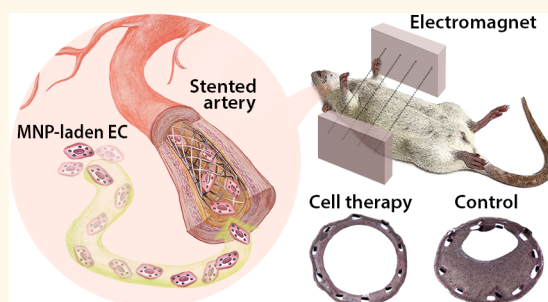
[∇]Department of Medicine, Division of Cardiology, Drexel University College of Medicine, Philadelphia, Pennsylvania 19102, United States

[#]Department of Surgery, Perelman School of Medicine, University of Pennsylvania, Philadelphia, Pennsylvania 19104, United States

[¶]Department of Electrical and Computer Engineering, Drexel University, Philadelphia, Pennsylvania 19104, United States

ABSTRACT: Although drug-eluting stents have dramatically reduced the recurrence of restenosis after vascular interventions, the nonselective antiproliferative drugs released from these devices significantly delay reendothelialization and vascular healing, increasing the risk of short- and long-term stent failure. Efficient repopulation of endothelial cells in the vessel wall following injury may limit complications, such as thrombosis, neoatherosclerosis, and restenosis, through reconstitution of a luminal barrier and cellular secretion of paracrine factors. We assessed the potential of magnetically mediated delivery of endothelial cells (ECs) to inhibit in-stent stenosis induced by mechanical injury in a rat carotid artery stent angioplasty model. ECs loaded with biodegradable superparamagnetic nanoparticles (MNPs) were administered at the distal end of the stented artery and localized to the stent using a brief exposure to a uniform magnetic field. After two months, magnetic localization of ECs demonstrated significant protection from stenosis at the distal part of the stent in the cell therapy group compared to both the proximal part of stent in the cell therapy group and the control (stented, nontreated) group: 1.7-fold ($p < 0.001$) less reduction in lumen diameter as measured by B-mode and color Doppler ultrasound, 2.3-fold ($p < 0.001$) less reduction in the ratios of peak systolic velocities as measured by pulsed wave Doppler ultrasound, and 2.1-fold ($p < 0.001$) attenuation of stenosis as determined through end point morphometric analysis. The study thus demonstrates that magnetically assisted delivery of ECs is a promising strategy for prevention of vessel lumen narrowing after stent angioplasty procedure.

KEYWORDS: magnetic nanoparticles, magnetic targeting, in-stent restenosis, endothelium, cell therapy, vascular healing



Progressive atherosclerosis causing luminal narrowing and obstruction in arteries is currently treated by a mechanical revascularization procedure known as stent angioplasty.^{1,2} However, this procedure is accompanied by severe arterial wall damage with concurrent endothelial denudation³ and inflammatory response,⁴ often leading to a recurrent blockage of the stented artery a condition known as in-stent restenosis.^{5,6} The key pathophysiologic factor responsible for restenosis after stenting is intimal hyperplasia, which is a result of the

proliferation and subsequent abluminal migration of vascular smooth muscle cells (VSMCs) that undergo a phenotypic switch from highly specialized contractile type to a synthetic or proliferative type in response to injury.³ Drug eluting stents (DESs) capable of delivering *in situ* potent antiproliferative

Received: July 22, 2016

Accepted: September 13, 2016

drugs significantly reduced the clinical incidence of restenosis in comparison with bare-metal stents, transforming the field of endovascular intervention.^{1,7} However, because DESs release nonselective drugs that do not discriminate between proliferating VSMCs and endothelial cells (ECs), the reconstitution of the injured luminal EC layer and subsequent vascular healing are substantially delayed and altered.^{8–11} In addition, recent evidence suggests that DESs impair EC function.^{12,13} These factors promote in-stent neointimal hyperplasia and very late stent thrombosis, the key contributors to late stent failure.^{14,15}

Efficient restoration of the functional endothelial lining has the potential to reestablish an antithrombotic luminal surface and effectively inhibit thrombosis and formation of neointima.^{11,16} Increased coverage of the stent strut surface by ECs correlates with decreased rates of thrombotic events in human autopsy^{17–19} and animal studies.⁹ Experimental inhibition of endothelial repair after denudation of the luminal surface has been shown to result in dramatically elevated rates of thrombosis,²⁰ while regeneration of endothelial lining in animal vascular injury models correlates closely with reduced or absent neointima formation.^{21,22}

Recognizing the therapeutic potential of reendothelialization as a cell-based strategy to promote repair of the injured vascular intima, several experimental approaches aiming to repopulate ECs at the site of injury have been studied. Approaches involving local placement of ECs on an endovascular stent by seeding stents with ECs^{23–25} or capturing endothelial progenitors from the bloodstream with antibodies attached to the stents,²⁶ however, did not demonstrate efficacy, safety, and feasibility for clinical applications due to injury of ECs caused by the balloon distention, small number of progenitor cells in circulation, or potential nonspecific capture of inflammatory cells. Local endovascular delivery of cultured ECs has been reported as well but is also restricted by the requirement for prolonged occlusion of blood flow and low cell engraftment at the injury site.^{27,28}

Magnetic targeting of ECs to the vessel wall is an intriguing and promising technique that has been applied to address the drawbacks of previous strategies. The feasibility of magnetic localization of ECs to stented blood vessels has been demonstrated using transiently²⁹ and permanently³⁰ magnetized vascular stents. A recent study demonstrated that magnetic EC delivery to transiently magnetized stents in a rat carotid artery stenting model enhanced capture, retention, and proliferation of ECs at the site of stent implantation.³¹ Circumferential

localization of ECs overexpressing endothelial nitric oxide synthase (eNOS) in the nonstented vessel has been shown to improve vascular function in a mouse carotid artery injury model.³² A circular Halbach array, which augments the magnetic field at its center, was used to demonstrate an increase in cell retention in nonstented vessels leading to a nonsignificant reduction of restenosis 3 weeks after cell delivery in a rabbit model.³³ These studies provide encouraging indications that magnetic targeting of ECs can offer an effective way for accelerated recovery of denuded endothelium in blood vessels and potentially mitigate pathological side-effects associated with mechanical injury after implantation of endovascular stents.

In the present study, we investigated the hypothesis that magnetically mediated delivery of syngeneic endothelial cells to transiently magnetized vascular stents will result in efficient cell homing and long-term retention with subsequent prevention or attenuation of experimental in-stent stenosis induced by mechanical injury in a rat carotid artery stent angioplasty model (Figure 1).

RESULTS

Stent Targeting via Systemic Cell Administration. Due to implementation advantages of utilizing an intravenous (iv) route of cell administration, we first characterized the biodistribution pattern of syngeneic rat aortic endothelial cells (RAECs) laden with biodegradable superparamagnetic nanoparticles (MNPs) and labeled with a lipophilic near-infrared (NIR) fluorophore injected *via* the tail vein. At 1 h after iv cell administration, 89% ± 9% of the totally administered cells were detected in the lungs irrespective of cell dose (Figure 2A), while at 6 h only 42% ± 6% (Figure 2B) of the cells remained in the lungs showing that a significant fraction of cells redistributed to the post-lung organs (17% ± 2% in liver, 30% ± 3% in spleen, 8.0% ± 0.7% in kidneys, and 2.6% ± 0.3% in heart).

The patterns of cell distribution were obtained by means of fluorescence that does not reflect cell viability. To assess whether detected cells in various organs were alive, we employed live bioluminescent imaging, injecting cells loaded with MNPs, labeled with a NIR fluorophore, and transduced with luciferase enzyme encoding adenovirus. Using whole body imaging, at 6 h after iv cell administration, live cells were detected only in the lungs (Figure 2C). Imaging of the excised organs confirmed the

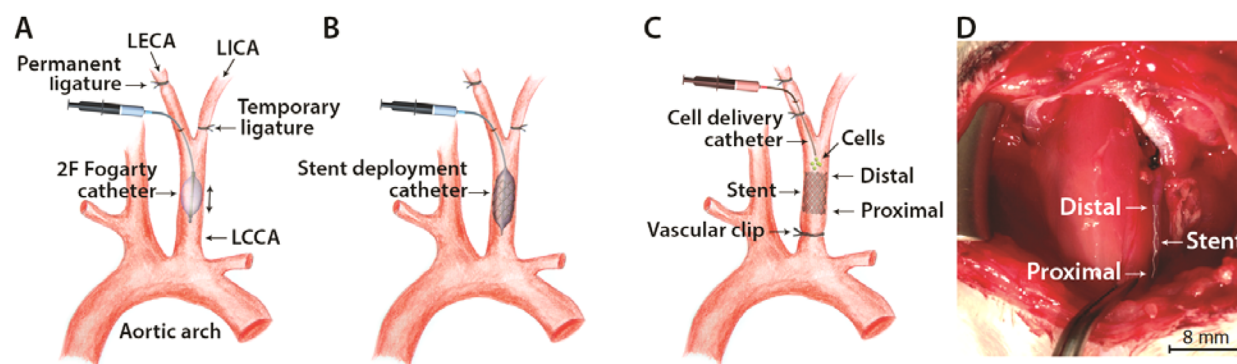


Figure 1. Rat carotid artery stent angioplasty model. (A) Injury of the common carotid is induced with four passages of the 2F Fogarty embolectomy catheter introduced through arteriotomy in the left external carotid artery (LECA) proximal to permanent ligature. Left internal carotid artery (LICA) is temporary ligated. (B) A bare-metal stent mounted onto an angioplasty catheter inserted into the midsection of the balloon injured left common carotid artery (LCCA) and deployed. (C) MNP-laden cells injected through a catheter positioned at the distal end of the implanted stent under stop-flow conditions (clamped common carotid artery). The excess of liquid is evacuated through the open left internal carotid artery. (D) Operative photograph of the stented left common carotid artery.

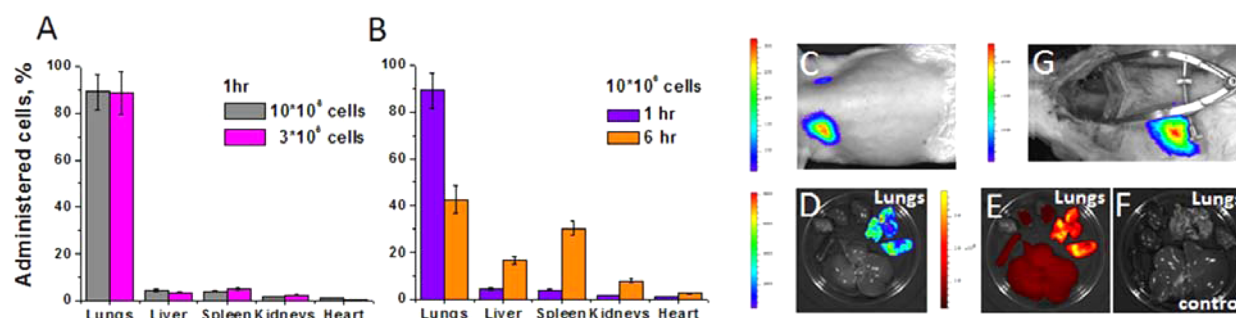


Figure 2. Cell biodistribution and stent targeting *via* systemic cell administration. The fluorescent and luminescent images were obtained using IVIS Lumina XR *in vivo* imaging system (PerkinElmer Inc.). (A) Biodistribution pattern (per fluorescence) of 3×10^6 and 10×10^6 cell doses at 1 h after intravenous (iv) cell administration; $n = 3$ for each group. (B) Biodistribution pattern (per fluorescence) of 10×10^6 cells at 1 and 6 h after iv cell administration; $n = 3$ for each group. (C) Live luminescent imaging of a Lewis rat 6 h after iv administration of 10×10^6 ECs loaded with MNPs, labeled with NIR-fluorescent dye, DiR, and transduced with luciferase-encoding adenovirus showing live cells only in the lungs. (D) Luminescent and (E, F) fluorescent images of the explanted organs showing live cells (per luminescence) in the lungs but not in the other post-lung organs; for panels C–F, $n = 3$. (G) Stent targeting experiment with iv administered ECs. Stented animals injected with 10×10^6 cells into the tail vein and exposed to a uniform magnetic field of 0.14 T for 45 min started at the time of cell injection did not show detectable cells in the stented artery segment, while showing presence of live cells only in the lungs; $n = 3$. Data represent the means \pm SD.

presence of live cells in the lungs, but not in other organs (Figure 2D). At the same time, fluorescence indicated the presence of cell-associated label in the post-lung organs (Figure 2E). Although these observations indicate that at most an extremely low fraction of viable cells can pass lung capillaries, we experimentally evaluated the possibility of capturing iv administered ECs on a stent implanted in carotid artery using tail vein administration of the ECs. Stented animals injected with 10×10^6 cells into the tail vein and exposed to the magnetic field for 45 min started at the time of cell injection did not have detectable cells in the stented artery segment, repeatedly showing the presence of live cells only in the lungs (Figure 2G). These experiments demonstrate that injection of RAECs *via* tail vein is not a suitable route for systemic cell administration to target stents implanted into rat carotid artery; therefore the next experiments were carried out using local delivery of cell therapy in a temporary isolated rat carotid artery (Figure 1) that has been shown to result in successful cell targeting to stents in our previous studies.²⁹

In Vivo Long-Term Cell Survival after Local Cell Delivery. To determine the cell dose for a local (at the stent) cell delivery setting, we estimated that about 100×10^3 cells can fully cover the accessible stent surface, assuming that the effective surface area of one EC is about $100 \mu\text{m}^2$ and the internal stent's surface is $\sim 10 \text{mm}^2$. To be able to inject $100 \mu\text{L}$ of cell suspension in the stop-flow setting, we kept an internal carotid artery branch open (Figure 1) to enable displacement of the added volume of cell suspension during magnetically guided delivery of cell therapy. Because the efficiency of targeting in the local cell delivery setting was unknown, we administered a 3-fold higher cell dose ($\sim 300 \times 10^3$ cells).

Bioluminescent imaging was used to confirm delivery of cell therapy and assess long-term cell survival over the two-month experimental time course. The first time point was evaluated at 1 week after cell delivery enabling animals to recover after the invasive procedure. At 1 week after cell delivery, about $(107 \pm 41) \times 10^3$ viable cells were detected in the stented artery segment, corresponding to $\sim 30\%$ of the totally administered cell dose in the local cell delivery setting (Figure 3A,E).

Interestingly, both the bioluminescent and fluorescent signals emitted by the targeted cells were asymmetrical, showing higher signal density at the distal part of the stent, the point where the

cell delivery catheter was positioned (Figure 3A,B). Additionally, the fluorescent signal (Figure 3B) validated cell localization in the stented artery segment eliminating the possibility of potentially free viral particles present in cell suspension that could transduce tissue of a recipient animal during local cell delivery. Two to three weeks post-cell delivery, the bioluminescent signal decreased ~ 2.5 -fold to a level of $\sim 40 \times 10^3$ viable cells staying stable until the animals were sacrificed (Figure 3C–E).

Progression of Vascular Treatment by Delivered Cells Monitored with Ultrasound. The progression of treatment of injured arteries with magnetically delivered ECs was monitored by high frequency ultrasound imaging measuring morphological (lumen diameter of the vessel with blood flow confirmed using B-mode and color Doppler flow imaging) and hemodynamic changes (peak systolic velocity (PSV), measured by quantitative pulsed wave Doppler mode) at the proximal and distal part of the stent. Animals with stented, mechanically injured arteries without cell delivery were used as control. Animals with cell delivery under nonmagnetic conditions were not included in this study because our earlier investigation showed that under nonmagnetic conditions the efficiency of cell delivery was about 10-fold inferior than under magnetic conditions.²⁹ Before injury, the normal diameters of the right carotid artery (used as internal control) and left carotid artery (implanted with a stent) were 1.09 ± 0.05 and 1.08 ± 0.04 mm, respectively ($n = 26$). Immediately after injury, the right carotid artery showed a transient drop in diameter, recovering to its nearly normal value with a nonsignificant 3% increase ($p > 0.05$) corresponding to 1.12 ± 0.04 mm 2 months later (Figure 4A). The transient drop in diameter could be a result of posttraumatic injury and effect of inflammation mediators (thromboxanes), while the subsequent increase seems to be a compensatory response due to decreased blood flow through the left common and external (permanently ligated) carotid artery. At the distal part of the stent, the control group showed marked $\sim 22\%$ reduction of luminal diameter, narrowing artery lumen to 0.85 ± 0.05 mm, while the diameter reduction in the cell therapy group was more moderate $\sim 13\%$, resulting in luminal narrowing to 0.95 ± 0.04 mm after 2 months (Figure 4A).

Contrastingly, quantitative analysis of the luminal diameter change at the proximal part of the stent did not show statistically significant differences in luminal narrowing between the cell therapy

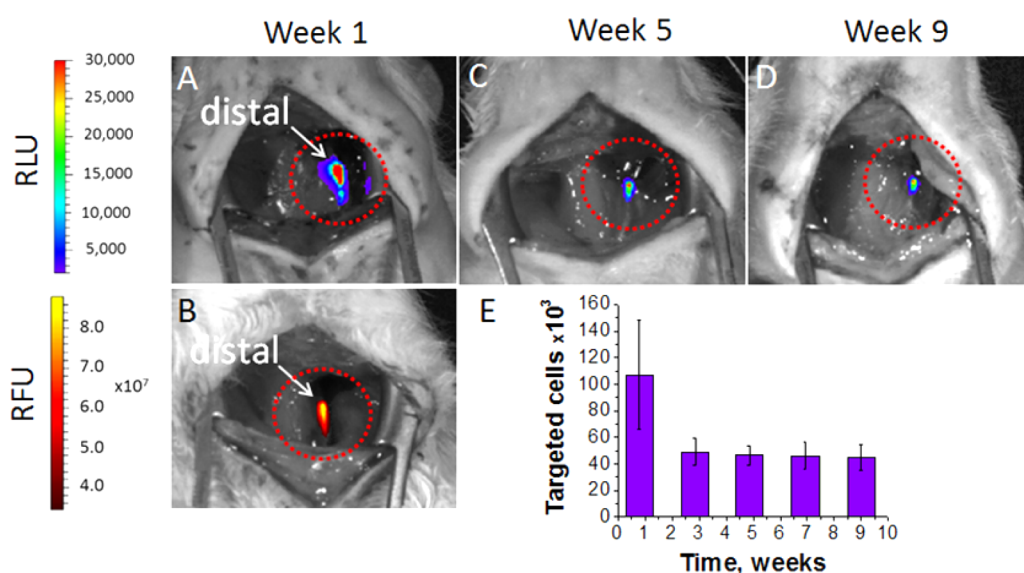


Figure 3. *In vivo* local magnetic cell delivery in a rat carotid stenting model under stop-flow conditions. The cells were loaded with MNPs, labeled with NIR-fluorescent dye (DiR), and transduced with luciferase-encoding adenovirus and administered at the distal end of the stent exposing the animal to a uniform magnetic field of 0.14 T generated across the neck area for 12 min. (A) Luminescent and (B) fluorescent signal emitted by the cells delivered to the stent 1 week after cell targeting. (C, D) Luminescent signal emitted by the originally delivered cells to the stented artery segment after 5 and 9 weeks postdelivery, respectively. (E) Numbers of the delivered cells over 9 weeks of the experimental time course, $n = 13$. Data represent the means \pm SD.

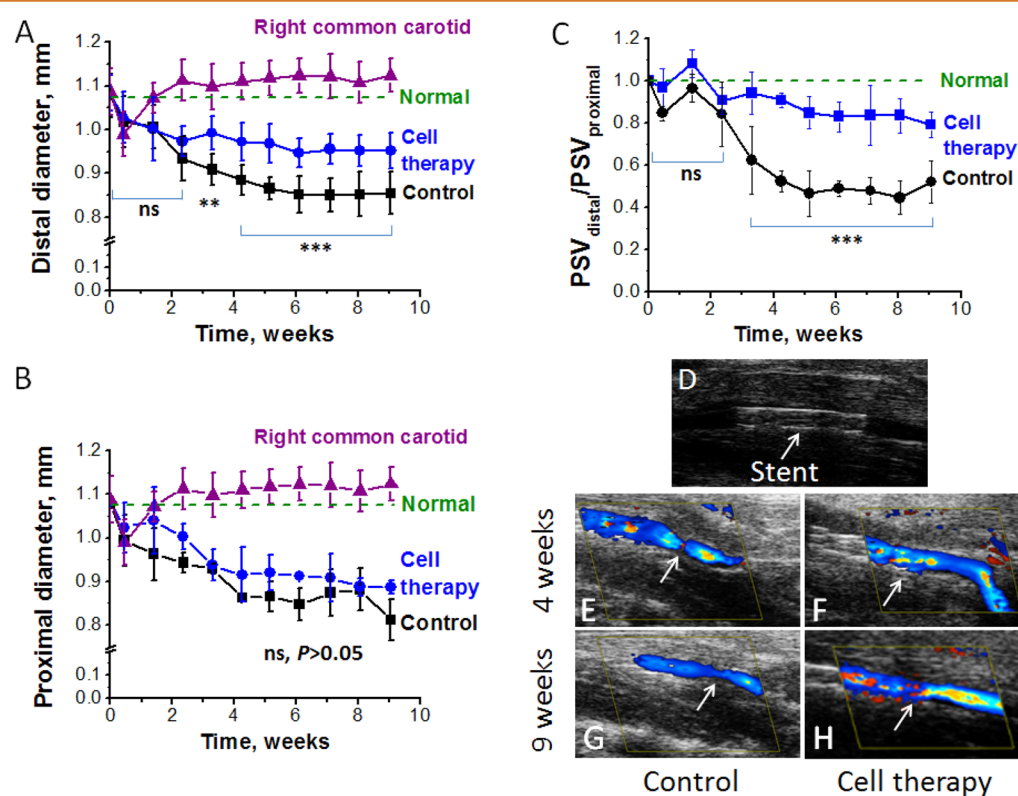


Figure 4. Protection from in-stent stenosis by the magnetically targeted ECs to the stented arteries assessed by the ultrasound. (A, B) Changes in diameter of the stented artery at the distal and proximal end, respectively ($n \geq 11$). (C) Ratios of the peak systolic velocity (PSV) at the distal to proximal ends in studied animal groups ($n \geq 11$). (D) B-mode ultrasound image of the stented left carotid artery. (E–H) Representative color Doppler images of the stented arteries at different time points. Arrows indicate distal end of the stented artery segment. Data represent the means \pm SD. Data comparisons were made using one-way analysis of variance (ANOVA) with Tukey's *post hoc* test; ** $p < 0.01$ and *** $p < 0.001$ versus untreated (control) arteries; ns, nonsignificant, $p > 0.05$. Normal are the values measured prior to stent implantation.

and control groups ($p > 0.05$) (Figure 4B). These results show a selective 1.7-fold ($p < 0.001$) greater protection from restenosis at the distal part of the stent in the cell therapy group compared to the proximal part of the stent.

Quantitative blood flow evaluation was based on pulsed wave Doppler measurement of peak systolic velocity (PSV), a hemodynamic parameter inversely proportional to the vessel's diameter in the power of four per corollary to the Poiseuille's law.

The normal PSV in the right and left carotid arteries was 937 ± 103 and 936 ± 150 mm/s, respectively ($n = 26$) (Figure 4C). In clinical practice, the absolute velocities in the internal common carotid (ICA) are usually normalized to the corresponding velocities in the ipsilateral common carotid artery (CCA) by generating ICA/CCA ratios. Such ratios are theoretically more robust measures because they may compensate for differences in clinical or physiological factors such as presence of tandem lesions, blood pressure, contralateral high grade stenosis, hyperdynamic cardiac state, or low cardiac output.^{34,35} Following this clinical standard, we compared ratios of $PSV_{\text{distal}}/PSV_{\text{proximal}}$ for each group, which represent ratios of velocities of the distal to proximal parts of the stented artery segment. The PSV ratios clearly indicate superior patency of the stented arteries in the cell therapy group, showing $\sim 21\%$ reduction in the normal ratio versus much more pronounced decrease to $\sim 48\%$ in PSV ratio in untreated, control group (Figure 4C). These results correlate well with the diameter changes showing 2.3-fold ($p < 0.001$) greater protection from restenosis in the cell therapy group. Throughout the study there were no episodes of stent thrombosis, and all the stented arteries remained patent to various degrees prior to euthanasia, as observed by the color Doppler flow imaging (Figure 4E–H).

Prevention of Restenosis by Targeted Cell Therapy Per Histological End Point Analysis. Morphometric analysis

showed that at the proximal and central part of the stented artery, intimal area was not statistically different ($p > 0.05$) between cell therapy and control animals as shown by percentage of stenosis (Figure 5A), neointima/media ratio (Figure 5B), and qualitative histological images (Figure 5E–G). However, at the distal part of the stented artery, cell delivery resulted in significant inhibition of in-stent stenosis with a prominent 1.8-fold ($p < 0.0001$) reduction in the percentage of stenosis ($40\% \pm 1\%$ vs $72\% \pm 11\%$) and 2.3-fold ($p = 0.0002$) reduction in the neointima/media ratio (1.54 ± 0.38 vs 3.18 ± 0.76) in cell therapy and control group, respectively (Figure 5A,B), which is also shown on the qualitative histological images (Figure 5C,D).

It is noteworthy, that in control animals, the greatest degree of stenosis was observed at the proximal and distal stent parts (edges) compared with the central part per both percentage of stenosis and neointima/media ratio. This result correlates closely with the modeling of balloon catheter inflation and stent expansion showing much more rapid and stronger expansion of the stent at the proximal and distal parts (edges) compared to the central part (Figure 6A,B).

Moreover, in control animals, the trend for significantly greater degree of stenosis was observed at the distal part of the stent compared to the proximal part resulting in percentage of stenosis of $72\% \pm 11\%$ and $52\% \pm 12\%$ ($p = 0.002$) or neointima/media ratio of 3.18 ± 0.76 and 2.36 ± 0.16 , ($p = 0.002$) respectively.

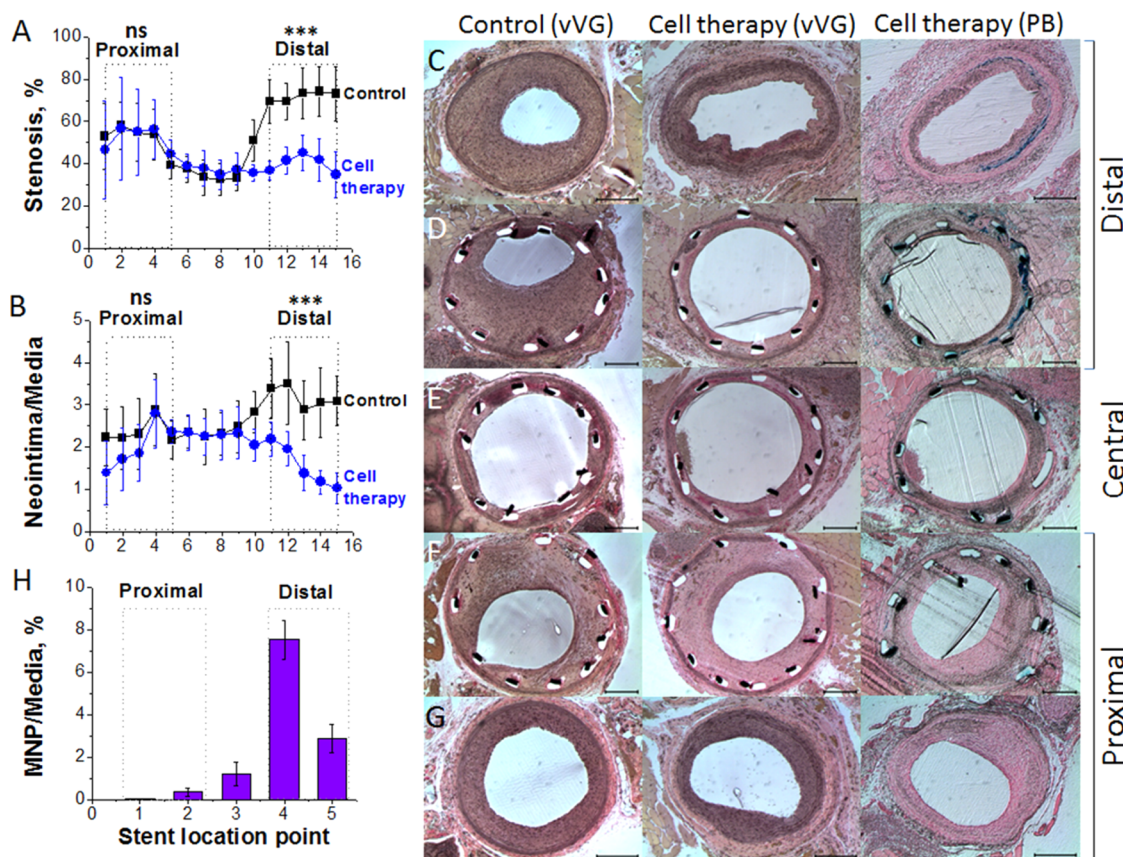


Figure 5. Protection from in-stent stenosis by the magnetically targeted ECs to the stented arteries assessed by morphometric analysis. The results expressed as (A) percent of stent stenosis and (B) neointima/media ratios along the stent ($n \geq 11$). (C–G) Representative Verhoeff-van Gieson (vVG) and Prussian blue (PB) with nuclear fast red as counterstain sections of stented arteries in control and cell therapy group at different stent location points. Blue staining in the Prussian blue-stained histological slices indicate presence of MNPs in the vessel wall. (H) Distribution of the MNPs along the stented artery segment quantified from the Prussian blue-stained histological slices. The scale is 0.25 mm. Data represent the means \pm SD. Data comparisons were made using two-tailed unpaired Student's *t*-test; *** $p < 0.001$ versus untreated (control) arteries; ns, nonsignificant, $p > 0.05$.

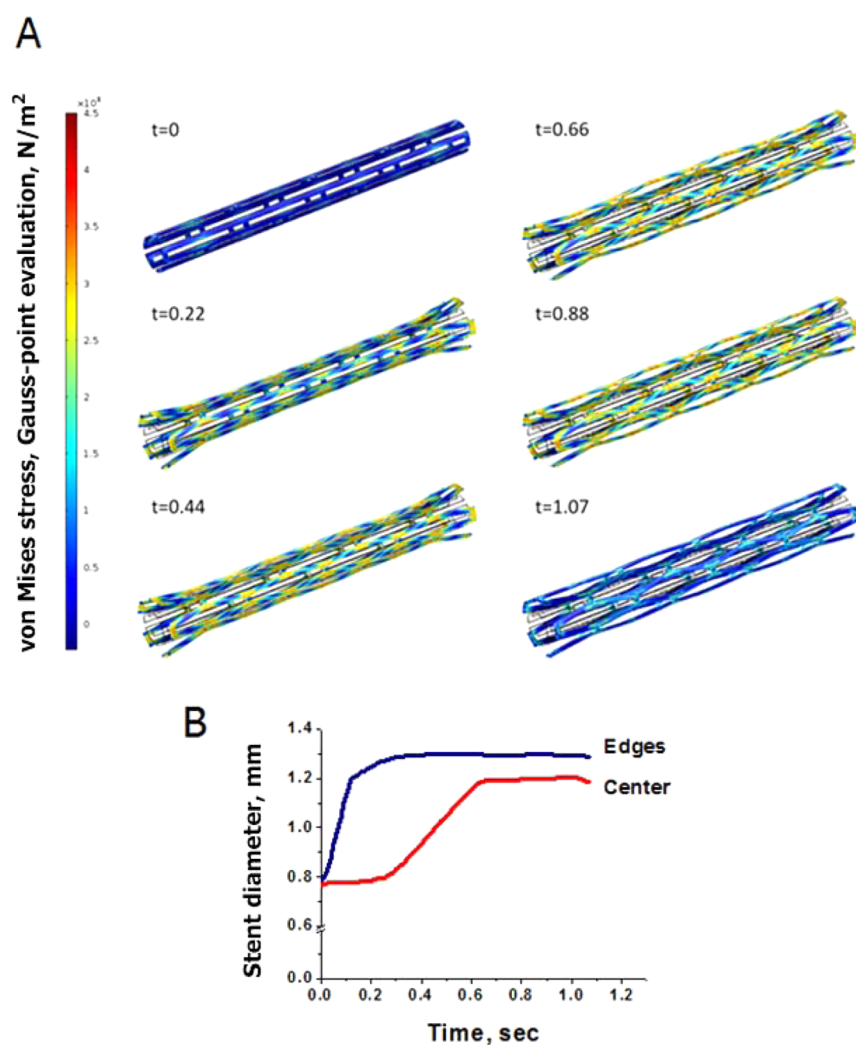


Figure 6. Illustration of the stent geometry during expansion. (A) The von-Mises stress within the stainless steel stent illustrated by a colored map. Six representative timeframes are demonstrated to show the differential expansion of the central and exterior sections (edges) of the stent. (B) The actual outer diameter of the central and the exterior parts (edges) of the stent are compared by plotting them *versus* the time of expansion. The COMSOL Multiphysics software (COMSOL Inc., Burlington, MA) was used to perform stent expansion modeling.

Consistently with morphometric and ultrasound data, traces of iron oxide nanoparticles were largely found at the distal part of the stented artery per quantitative Prussian Blue (PB) staining, confirming selective localization of the delivered cells at the distal part of the stent (Figure 5C–E, cell therapy (PB) panel).

DISCUSSION

Endothelial denudation and dysfunction are considered to be primary traumatic sequelae of endovascular interventions, often leading to an acute thrombosis and restenosis. Clinically used DESs, although significantly reducing the incidence of restenosis, result in substantially delayed reendothelialization due to release of nonselective drugs that inhibit both VSMCs and ECs in the injured vessel.⁹ The prolonged impairment of endothelial regeneration, critical to vascular healing, directly contributes to objectionably high rates of late thrombosis and neoatherosclerosis.^{11,15} Early restoration of endothelial integrity has been shown to modify thrombogenic and proliferative vascular wall properties in a number of animal models.^{36,37} These observations motivated us to test the hypothesis that accelerating endothelium recovery may prevent postangioplasty complications and improve long-term patency of vascular stents. In this study, we assessed the

potential of magnetically guided delivery of syngeneic ECs to inhibit experimental in-stent stenosis induced by mechanical injury in a rat carotid artery stent angioplasty model.

The targeted cell delivery strategy implemented in this study utilizes a uniform magnetic field capable of penetrating deeply into the body in combination with a magnetizable implant (endovascular stent) to magnetize ECs laden with superparamagnetic nanoparticles (MNPs) only during the time of the field application and generate high field gradients localized in the proximity to the steel stent wire network resulting in an attractive force facilitating targeting of MNP-laden ECs at the site of stent implantation. The main advantage of this approach is in using modest (below 0.2 T) external uniform magnetic field for realization of magnetically mediated cell delivery^{29,31} or other types of therapies^{38,39} that can be implemented even in deep anatomical sites of the human body. Generation of such modest uniform magnetic fields across large animals or even humans is feasible (either by use of large custom designed electromagnets or MRI devices), as opposed to situations where gradient fields are used for the same purpose. This distinction makes our approach highly attractive for the future clinical translation. Since the stent and MNPs do not retain remnant magnetization after

the external field is removed (due to superparamagnetic properties), any problems associated with retaining permanently magnetic objects within the patient are eliminated. If redosing of therapy is required, the stent can be remagnetized through the application of an external uniform magnetic field and the therapy delivery procedure repeated.

To test our hypothesis that prompt targeted delivery of ECs to stented arteries can attenuate experimental in-stent stenosis, we used laboratory rats as the smallest and most cost-effective animals that enable direct implantation of a stent in the carotid artery.^{29,40–43} The use of autologous cells in the long term therapeutic efficacy studies is an ideal strategy to eliminate immunological rejection of the delivered cells by the host. However, rats are too small for the generation of autologous vascular ECs. Therefore, the current therapeutic efficacy study was conducted using inbred Lewis rats and syngeneic primary aortic ECs isolated from closely related individuals. The syngeneic cells used in this study represented a highly pure culture of ECs (98% CD31⁺, 90% Tie-2⁺, and 4% α -SMA⁻ (SMA = smooth muscle actin) per flow cytometry)⁴⁴ that were tolerated well by all the recipient animals. It is noteworthy that the internalization of polymeric MNPs used in this study to confer cells with magnetic responsiveness for achieving efficient targeting was accomplished by loading an individual cell on average with ~ 25 pg of magnetite. This did not markedly affect cell functional competence, gene expression, intracellular organelles, or cell respiration.^{44,45}

The results from our previous study demonstrated the feasibility of magnetic guidance to target (model) ECs to stented rat carotids mediated by a uniform magnetic field. ECs administered into the left ventricular cavity *via* intracardiac injection were uniformly captured from systemic circulation onto the stent struts.²⁹ Due to noncompatibility of traumatic intracardiac injections with a long-term survival experiment, we evaluated the possibility of an alternative systemic administration of ECs. Since all accessible arteries in rats are downstream of carotids, the only feasible method for systemic cell administration was *via* the tail vein. Because recent data suggested that the majority of intravenously administered mesenchymal stem cells (MSCs) are initially trapped inside the lung capillaries (the pulmonary “first-pass” effect)^{46,47} with only a few cells reaching the area of injury, we evaluated the feasibility of iv cell administration in our specific case. Although per fluorescence we observed cell-associated label in the post-lung organs at 1 h and more profoundly at 6 h post-cell administration, the bioluminescent imaging indicated that this signal did not represent live cells that apparently were able to pass the lung barrier. Consistent with this observation from the biodistribution experiments, no viable cells were captured on stents in magnetic targeting experiments involving iv cell administration (Figure 2G). In contrast, in the stop-flow setting of local cell delivery, we observed significant numbers of ECs present in the stented artery segment 1 week after cell delivery, corresponding to $\sim 30\%$ of the initially administered cell dose, which may be a result of multifactorial effects due to cell replication and transient expression of luciferase transgene, typical to adenoviral vectors. Notably, the asymmetric shape of both bioluminescent and fluorescent signals (Figure 3A,B) indicates a non-uniform cell distribution, with preferential cell accumulation at the distal part of the stented artery, the point of positioning of a cell delivery catheter. Sustained cell homing and engraftment in the stented artery tissue was evidenced by a persistent bioluminescent signal detected 3–9 weeks post-cell delivery, while marked ~ 2.5 -fold

reduction of cell number may be a result of partial cell loss or transient expression of luciferase transgene. A recent study involving largely similar animal model and targeting conditions demonstrated that syngeneic RAECs delivered at ~ 30 -fold lower cell dose compared to the current study expanded over 1 week after targeting.³¹ Because EC proliferation is intrinsically exemplified by contact inhibition, future efficacy studies will need to be conducted to carefully optimize cellular dose accounting for cell proliferation and the shortest possible time-frame for achieving fully reendothelialized stented artery tissue.

High frequency ultrasound allowed us to determine the patency of stented arteries and identify potential thrombotic events and also enabled us to noninvasively monitor the progression of the induced disease along with treatment in the studied animals. Remarkably, the ultrasound observations indicated a selective partial therapeutic effect due to magnetically localized ECs at the distal part of the stented artery per both morphological and hemodynamic parameters (Figure 4A–C), consistent with bioluminescent imaging. Dissection of the entire segment of the stented artery in histological samples clearly validated this observation, demonstrating marked antirestenotic effect at the distal part of the stent, consistent with the visible presence of MNP traces at the distal part of the stent and the adjacent artery (Figure 5C–E, cell therapy (PB) panel). It is interesting to note that in the control group, the greatest extent of neointimal tissue was present at the proximal and distal regions of the stent, which agrees with findings in animal^{48,49} and clinical studies.⁵⁰ Our stent expansion model (Figure 6A,B) demonstrates that a stent expands more rapidly and to a greater extent at the ends (edges) rather than along the axis from the ends. This indicates a potentially greater stress concentration applied by the stent to the artery wall at the edges, where the elastic properties of the two materials are mismatched.⁵¹ Proliferation of VSMCs in the media and neointima seem to be an adaptive response to compliance mismatch that exists in regions of stress concentration, thereby leading to stronger restenosis at the stent ends. In addition to the edge phenomenon observed in control animals, the extent of neointimal thickening was greater at the distal part comparing to proximal. This result points out that a greater degree of injury at the distal part of the stented artery segment may be an effect of a higher traffic of catheters introduced in close proximity to the distal part of the stented artery through the external carotid during stenting and cell delivery procedures.

Despite the expected stronger injury at the distal end, as was observed in the control animals, magnetically assisted delivery of ECs markedly attenuated this effect in the same site of the treatment group animals, indicating that repopulation of ECs recreated a microenvironment promoting vascular healing at the site of the stronger injury. The partial nature of the antirestenotic effect in our local cell delivery setting seems to be reasonably attributed to a nonuniform targeting of ECs, creating a gradient of conditions in the vessel wall and translating into incomplete vascular healing of the entire stented artery segment. Although this situation may be regarded as one of the nonanticipated study limitations, we recognize this outcome as demonstrating built-in dose-dependence, showing that the lack of protection from in-stent stenosis is caused by incomplete coverage of ECs. This view, in our opinion, strengthens our observations supporting that therapeutic effect was selectively promoted at the artery site that was successfully repopulated with ECs.

Cell delivery at the distal end of the stent under stop-flow conditions, though suboptimal, was the only experimentally

feasible approach due to the small size of the rat anatomy. We assume that the following reasons can explain the selective cell localization at the distal part of the stent. First, injecting a cell suspension into a ~ 1 mm stented blood vessel under interrupted blood flow condition (clamped common carotid) may not create a flow pattern enabling all the cells to pass through the stent resulting in uniform distribution of cells. Second, cells delivered at the distal end are likely to experience the highest field gradient at the stent's edge attracting most of the delivered cells to the distal part of the stent.

While the bioluminescent data indicates that only a fraction of the originally delivered ECs was still viable 2 months post-cell delivery, due to transient cell transduction with luciferase transgene, the proliferation potential of the delivered cells could not be assessed with this technique. Additionally, for technical reasons, we were not able to specifically stain ECs in histological samples to obtain a morphological picture of EC localization in the stented artery wall. These limitations did not allow us to make definitive conclusions regarding the reendothelialization in the studied animals. Despite these limitations, ultrasound measurements of both artery diameter reductions at the distal end (Figure 4A) and PSV ratios (Figure 4C) show that the progression of in-stent stenosis halts after ~ 1.5 and 3.3 weeks (per diameter, $p > 0.05$ after these time-points) and after ~ 2.4 and 4.3 weeks (per PSV ratios, $p > 0.05$ after these time points) in cell therapy and control animals, respectively, demonstrating that magnetically mediated targeting of non-modified ECs prevented development of in-stent stenosis nearly 2-fold earlier and with 2-fold greater magnitude in treated animals in comparison to untreated controls.

In the future clinical setting, uniform cell delivery to stented arteries can be achieved immediately after stent deployment by administering cells through the delivery channel of the stent deploying catheter or post-dilatation balloon catheter under fluoroscopy, gradually drawing the catheter from one end to another end of the stented artery segment without occlusion of the blood vessel. From a clinical perspective, a few additional important issues should be addressed for translation of the magnetic targeting methodology. In this study, we used stents made of 304-grade stainless steel, which is not approved by the Food and Drug Administration (FDA) for vascular applications due to inferior corrosion resistance compared to clinically used stents made of 316L-grade stainless steel. The cold working process by changing the microstructure of the stainless steel can be potentially used to increase magnetic permeability of the 316L stainless steel. Alternatively, if the proposed magnetic cell targeting methodology will offer significant improvements in long-term stent performance, substantially reducing clinical complications associated with currently used stents, the inferior corrosion resistance may be outweighed, providing the rationale for clinical approval of the 304-grade stainless steel. To avoid potential immunologic/rejection problems, the proposed methodology would require the patient to be the autologous donor for the ECs. We envision that in the future, the technologies will further evolve to safely transform patient's cells into induced pluripotent cells (iPS), which can be controllably differentiated into ECs or any other cell type that can be used for regenerative needs. Having a technology to preserve cells isolated from a person until the potential health risk for the person is identified, the preserved autologous cells can be prepared for a planned medical treatment in advance.

CONCLUSIONS

Recurrent arterial narrowing and late stent thrombosis after mechanical injury caused by stent implantation remain the Achilles' heel of endovascular intervention. Current standards of clinical care focus on inhibition of smooth muscle cells using drug-eluting stents that release nonselective antiproliferative drugs, which also affect endothelial cells, the important modulators of vascular hemostasis, fibrinolysis, and proliferative state of the smooth muscle cells. Alternatively, the promotion of healing in the vascular endothelium may be a more natural and consequently safer approach in the prevention of vascular restenosis and thrombosis. This work demonstrates that magnetically mediated targeting of nonmodified endothelial cells prevented development of in-stent stenosis nearly 2-fold earlier and with 2-fold greater magnitude in treated animals in comparison to untreated controls. In the future, addressing uniformity of cell delivery, choice of stent material, cell source and considering enhancement of EC function *via* genetic manipulation, the methodology investigated here may provide the basis for designing the next generation of cell-based therapy for vascular healing after stent angioplasty. Thus, the potential therapeutic value, safety, and feasibility of the approach presented here merit further investigation.

METHODS

Nanoparticles and Cell Preparation. Polylactide-based magnetic nanoparticles were formulated with inclusion of nanocrystalline magnetite by a modified emulsification–solvent evaporation method as described elsewhere.^{52,53} The particles contained $48.2\% \pm 1.32\%$ (w/w) magnetite (per spectrophotometry) and were fluorescently labeled by boron-dipyromethene (BODIPY) 650/665 nm (Thermo Fisher Scientific, Rockford, IL, USA) as described elsewhere.⁵⁴ The MNPs had a mean hydrodynamic diameter of 278 ± 1.62 nm and ζ -potential of -14.4 ± 0.34 mV. Magnetization of the MNPs measured at 0.5 T was 24.6 ± 1.22 emu/g of composite. Full physicochemical characterization of MNPs can be found in ref 52.

Rat aortic endothelial cells (RAECs) were isolated and characterized according to previously published protocol.⁴⁴ For cell loading, RAECs were seeded on clear-bottom 12-well plates (BD Biosciences, USA) using MCDB 131 medium supplemented with 5% fetal bovine serum (FBS), epidermal growth factor (EGF) (10 ng/mL), hydrocortisone (1 μ g/mL), and L-glutamine (10 mM). The original MNP suspension (20 μ L, an equivalent of 0.736 mg) was dispersed in 10 mL of the cell culture medium and filtered through a Millipore syringe driven filter with 5.0 μ m pores. The MNP suspension was given to cells in the volume of 2 μ L (0.0736 mg) of MNPs per 300 000–350 000 cells (a given dose of ~ 100 pg of magnetite/cell for 48% w/w MNPs) and incubated at 37 °C for 24 h on a 96-well magnetic separator with surface force density of 66 T²/m (LifeSep 96F, Dexter Magnetic Technologies, USA). The cells were washed three times with PBS to remove noninternalized particles. Then, cells were trypsinized and resuspended in PBS for further use in *in vivo* experiments. After overnight incubation of cells with particles on a magnetic separator, the magnetite content within RAECs was estimated to be 25.3 ± 0.75 pg of magnetite/cell as quantified by the method described elsewhere.⁵⁵

Cell Biodistribution Studies. For biodistribution studies, MNP-loaded cells were labeled with a lipophilic near-infrared (NIR) fluorescent probe (DiR from Thermo Fisher Scientific, Rockford, IL, USA) in order to minimize the fluorescence background of the animal tissue in the visible range.⁵⁶ Upon completion of MNP-loading, the cells were trypsinized, centrifuged for 5 min at 1000 rpm, resuspended in 2 mL of MCDB131 medium supplemented with 16 μ g/mL of DiR, and incubated for 45 min in the tissue culture incubator. Thereafter, the labeled cells were washed twice with 10 mL of PBS, with centrifugation for 5 min at 1000 rpm between the washes. After the final wash, the cells were counted and resuspended in PBS to generate two cell doses at a final concentration of 3×10^6 and 10×10^6 cells/300 μ L.

For bioluminescent measurements, the cells were additionally transduced with luciferase enzyme encoding, replication defective adenovirus (Vector Core Facility, University of Pennsylvania, PA, USA) at multiplicity of infection (MOI) = 2000 at which we achieved maximal transduction efficiency without adversely affecting cell viability.

All animal studies were performed with the approval and according to the guidelines of the Institutional Animal Care and Use Committee of the Drexel University, College of Medicine, PA, USA. A total of 12 male Lewis rats with body weight of 350–400 g (Envigo, East Millstone, NJ, USA) were used in biodistribution studies. The cell preparations were injected into the tail vein of rats at a rate of 0.67×10^6 cells/min. At 1 and 6 h after cell administration, the animals were euthanized, and organs were collected for NIR fluorescent measurements (710–760 nm and 810–875 nm excitation and emission passbands, respectively) using IVIS Lumina XR *in vivo* imaging system (PerkinElmer Inc., Waltham, MA, USA). The total radiant efficiency measured for each organ from both sides was normalized to the organ mass. The cell fraction contained within each organ was obtained as a ratio of the fluorescence from a particular organ to the total fluorescence from all the organs and presented as a percent of the total administered cells. In bioluminescent biodistribution experiments, the D-Luciferin Firefly potassium salt (PerkinElmer Inc. USA) was administered into a tail vein at a dose of 150 mg/kg per manufacturer protocol prior to the imaging. The collected bioluminescent signal was integrated over 5 min. Living Image Software, version 4.3.1, PerkinElmer Inc., was used to analyze the obtained imaging data.

Stent Angioplasty and *in Vivo* Cell Delivery. A total of 29 male Lewis rats (26 for local cell delivery and 3 for tail vein cell administration) with body weight of 450–500 g were used from Envigo, East Millstone, NJ, USA. Animals were started on antiplatelet therapy (aspirin, 30 mg/L in drinking water) 2–3 days before surgery, and this therapy continued for 1 week. Under general anesthesia (2–3% isoflurane) prior to surgery, the animals were injected with subcutaneous (sc) meloxicam (1 mg/kg), intramuscular (im) cefazolin (20 mg/kg), and intraoperatively following vascular dissection with iv heparin (200 units/kg). The supplemental fluids (20 mg/(kg-h), iv) were infused during the surgical procedure. Left common carotid arteries along with external and internal carotids were isolated with blunt dissection. The external carotid was permanently ligated as distal as possible. The proximal part of the common carotid and internal carotid were temporary occluded with vascular clip and temporary ligature, respectively. Injury of common carotids was induced with four passages of 2F Fogarty embolectomy catheter (Edwards Lifesciences, Irvine, CA, USA) introduced through arteriotomy in external carotid proximal to ligation (Figure 1A). A 304-grade stainless steel stent (Lasera Technology Corp. Waukegan, IL, USA) was introduced into common carotid through the conductor tube inserted in external carotid and deployed at the injured artery segment with angioplasty balloon catheter (NuMED Inc., Hopkinton, NY, USA) applying hydrostatic pressure of 12 atm for 20 s (Figure 1B). This procedure is visually described elsewhere.⁴² In control animals ($n = 13$), the procedure was completed with permanent ligation of the external carotid distal to common carotid bifurcation, blood flow was restored, and the wound was closed. In cell delivery animals ($n = 13$), a 26 gauge First PICC S/L catheter (Argon Medical Devices Inc. Plano, TX, USA) prefilled with a suspension of MNP-laden RAECs was introduced and affixed by ligature on external carotid keeping the tip of the catheter at the distal end of the stent. The temporary ligature on the internal carotid was released to allow liquid evacuation during the injection of cells (Figure 1C). The animal was transferred and positioned between the poles of a C-core electromagnet with a 4 cm gap and 100 μ L of 3×10^5 cells/ μ L was injected at a rate 50 μ L/min exposing the animal to a uniform magnetic field of 0.14 T generated across the neck area by two symmetrical electromagnets for 12 min. After cell delivery procedure, the catheter was removed, the external carotid was tied off distally to the common carotid bifurcation, blood flow was restored by removing the clamp and temporary ligature (Figure 1D), and the wound was closed. Animals were monitored for body weight changes and signs of general well-being and were administered antibiotics (cefazolin) and analgesia (meloxicam) daily over 3 days after the surgical procedure using doses described above.

Imaging Studies. One week and subsequently 3, 5, 7, and 9 weeks after magnetic cell delivery, the animals of the treatment group were subjected to bioluminescent and fluorescent imaging to track delivered cells (IVIS Lumina XR, PerkinElmer Inc., Waltham, MA, USA). Bioluminescent imaging involved local application under general anesthesia of 100 μ L of D-Luciferin (30 mg/mL) admixed with 250 μ L of 37.5% (w/v) Pluronic F127 (Sigma-Aldridge, St. Louis, MO, USA) solution applied to the external surface of the stented common carotid. The bioluminescence data acquisition started immediately after application of the luciferase containing gel using 5 min integration time.

For ultrasound imaging, under general anesthesia the animal was placed on the study platform of the Vevo2100 Imaging System (VisualSonics Toronto, ON, Canada) in dorsal position with extremities taped to the electrodes for ECG tracing. After general visualization in B-mode to locate the stented and contralateral carotid arteries, images were recorded for subsequent diameter measurements in selected control zones of the stented segments of left common carotid artery (proximally to the stented segment, most proximal, the most distal, and immediately distally to the stented segment). Presence of blood flow and its nonquantitative evaluation were conducted in color Doppler mode with 250 MHz probe positioned at 60° angle to the studied vessel. Evaluation was based on the shape, color scale, and homogeneity of the flow image. For quantitative analysis of peak systolic velocity (PSV), pulsed wave Doppler mode recordings were conducted at the same control zones of left common carotid arteries as for diameter measurements making sure of the optimal probe positioning based on the color Doppler image. Recordings in the same modes were conducted at the corresponding 10 mm length area of right common carotid artery proximately to its bifurcation as control site. Cardiac and respiratory functions of the tested animal were monitored during ultrasound recording to ensure acquisition of true measurements. The ultrasound recordings were done before surgery and weekly after stenting and cell delivery procedure.

Morphometric Analysis. Approximately 64 days post-stent implantation and cell delivery procedure (64 ± 1 day), animals were euthanized. During the necropsies, the stented arteries were located, flushed with PBS, and fixed *in situ* by perfusion with 10% neutral buffered formalin. The stented arterial segments were glycol methacrylate embedded (JB-4, Electron Microscopy Sciences, PA, USA). Serial 5- μ m cross sections were obtained at subsegmental intervals of 100–200 μ m using rotary microtome HM355S (Microm International, Germany) equipped with a tungsten carbide knife (Delaware Diamond Knives, DE USA). Cross sections were stained by Verhoeff–van Gieson elastin stain or by Prussian blue staining with nuclear fast red as counterstain. The morphometric analysis was performed using ImageJ software (version 1.43, NIH) by an observer blinded to the study groups. The morphometric analysis was performed to measure the areas inside the lumen, internal elastic lamina (IEL) and external elastic lamina (EEL). Measurements allowed for calculation of intimal area (IEL area – lumen area) and medial area (EEL area – IEL area) and subsequently for neointima/media ratio and percent stenosis [$1 - (\text{lumen area}/\text{IEL area}) \times 100\%$].⁵⁷ The distribution of MNPs was analyzed by the ImageJ software measuring area occupied by MNPs from the Prussian blue stained slices and presented as a percent relative to the area of the media.

Stent Expansion Modeling. In order to determine the stent geometry during its expansion, we used COMSOL Multiphysics software (COMSOL Inc., Burlington, MA). For symmetrical reasons, it was sufficient to model only 1/20 of the stent's geometry. The stent is comprised of cold-worked 304 grade stainless steel, and the Young's modulus was set to 196 GPa,⁵⁸ the Poisson's ratio to 0.27,⁵⁸ the initial yield stress to 277 MPa,⁵⁹ the density to 7955 kg/m³,⁵⁸ and isotropic tangent modulus to 692 MPa.⁶⁰ We used the solid mechanics modulus, while a radial outward pressure was applied on the inner surface of the stent to represent the expansion of a balloon. In order to simulate the balloon-derived pressure, the load was represented with a step function; the load was set to drop to zero as soon as the inner radius of the stent was higher than the preset radius of 0.547 mm. Due to the highly nonlinear nature of this model, a displacement control parameter was used to improve the convergence during the computation of the

solution. Here, the average displacement of the stent's inner radius is prescribed, and a global equation is used to compute the corresponding applied pressure load.

Statistical Analysis. Data are expressed as means \pm SD (standard deviation). Statistical calculations were performed with GraphPad Prism 5 (Graphpad, La Jolla, CA). Statistical tests used to compare the differences are specified in the figure legends. The data were tested for normality by the Shapiro–Wilk method; p values of <0.05 were considered significant. In ultrasound or histology analyses, a few replicates were not included due to poor signal or sample quality (n specified in the figure legends).

AUTHOR INFORMATION

Corresponding Author

*E-mail: bpolyak@drexelmed.edu.

Author Contributions

[‡]B.P. and M.M. contributed equally. B.P. and M.M. designed research; B.P., M.M., N.L., L.S., A.R., M.Y.R., and K.W. performed research, B.P., M.M., N.L., L.S., T.P., A.R., M.Y.R., A.R.K., R.S., and G.F. analyzed data; B.P., M.M., L.S., A.R.K., R.S., and G.F. wrote the paper.

Notes

The authors declare no competing financial interest.

ACKNOWLEDGMENTS

This work was supported by the National Heart, Lung, and Blood Institute Award R01HL107771, W.W. Smith Charitable Trust Award H1504, Drexel University College of Medicine Clinical & Translational Research Institute (CTRI), Office of Research, Drexel University (IVIS grant), and Commonwealth of Pennsylvania Universal Research Enhancement (CURE) grant to B. Polyak. We thank Y. Saint-Etienne for assistance with the illustrations.

REFERENCES

- (1) De Luca, G.; Dirksen, M. T.; Spaulding, C.; Kelbaek, H.; Schlij, M.; Thuesen, L.; van der Hoeven, B.; Vink, M. A.; Kaiser, C.; Musto, C.; Chechi, T.; Spaziani, G.; Diaz de la Llera, L. S.; Pasceri, V.; Di Lorenzo, E.; Violini, R.; Cortese, G.; Suryapranata, H.; Stone, G. W. Drug-Eluting vs. Bare-Metal Stents in Primary Angioplasty: A Pooled Patient-Level Meta-Analysis of Randomized Trials. *Arch. Intern. Med.* **2012**, *172*, 611–621.
- (2) Stefanini, G. G.; Holmes, D. R., Jr. Drug-Eluting Coronary-Artery Stents. *N. Engl. J. Med.* **2013**, *368*, 254–265.
- (3) Chaabane, C.; Otsuka, F.; Virmani, R.; Bochaton-Piallat, M. L. Biological Responses in Stented Arteries. *Cardiovasc. Res.* **2013**, *99*, 353–363.
- (4) Kornowski, R.; Hong, M. K.; Tio, F. O.; Bramwell, O.; Wu, H.; Leon, M. B. In-Stent Restenosis: Contributions of Inflammatory Responses and Arterial Injury to Neointimal Hyperplasia. *J. Am. Coll. Cardiol.* **1998**, *31*, 224–230.
- (5) Alfonso, F.; Byrne, R. A.; Rivero, F.; Kastrati, A. Current Treatment of In-Stent Restenosis. *J. Am. Coll. Cardiol.* **2014**, *63*, 2659–2673.
- (6) Kim, M. S.; Dean, L. S. In-Stent Restenosis. *Cardiovasc. Ther.* **2011**, *29*, 190–198.
- (7) Marks, A. R. Sirolimus for the Prevention of In-Stent Restenosis in a Coronary Artery. *N. Engl. J. Med.* **2003**, *349*, 1307–1309.
- (8) Guagliumi, G.; Sirbu, V.; Musumeci, G.; Gerber, R.; Biondi-Zoccai, G.; Ikejima, H.; Ladich, E.; Lortkipanidze, N.; Matiashvili, A.; Valsecchi, O.; Virmani, R.; Stone, G. W. Examination of the *In Vivo* Mechanisms of Late Drug-Eluting Stent Thrombosis: Findings from Optical Coherence Tomography and Intravascular Ultrasound Imaging. *JACC Cardiovasc. Interv.* **2012**, *5*, 12–20.
- (9) Joner, M.; Nakazawa, G.; Finn, A. V.; Quee, S. C.; Coleman, L.; Acampado, E.; Wilson, P. S.; Skorija, K.; Cheng, Q.; Xu, X.; Gold, H. K.; Kolodgie, F. D.; Virmani, R. Endothelial Cell Recovery between

Comparator Polymer-Based Drug-Eluting Stents. *J. Am. Coll. Cardiol.* **2008**, *52*, 333–342.

(10) Kotani, J.; Awata, M.; Nanto, S.; Uematsu, M.; Oshima, F.; Minamiguchi, H.; Mintz, G. S.; Nagata, S. Incomplete Neointimal Coverage of Sirolimus-Eluting Stents: Angioscopic Findings. *J. Am. Coll. Cardiol.* **2006**, *47*, 2108–2111.

(11) Otsuka, F.; Finn, A. V.; Yazdani, S. K.; Nakano, M.; Kolodgie, F. D.; Virmani, R. The Importance of the Endothelium in Atherothrombosis and Coronary Stenting. *Nat. Rev. Cardiol.* **2012**, *9*, 439–453.

(12) Fuke, S.; Maekawa, K.; Kawamoto, K.; Saito, H.; Sato, T.; Hioka, T.; Ohe, T. Impaired Endothelial Vasomotor Function after Sirolimus-Eluting Stent Implantation. *Circ. J.* **2007**, *71*, 220–225.

(13) Maekawa, K.; Kawamoto, K.; Fuke, S.; Yoshioka, R.; Saito, H.; Sato, T.; Hioka, T. Severe Endothelial Dysfunction after Sirolimus-Eluting Stent Implantation. *Circulation* **2006**, *113*, e850–e851.

(14) Nakazawa, G.; Otsuka, F.; Nakano, M.; Vorpahl, M.; Yazdani, S. K.; Ladich, E.; Kolodgie, F. D.; Finn, A. V.; Virmani, R. The Pathology of Neoatherosclerosis in Human Coronary Implants Bare-Metal and Drug-Eluting Stents. *J. Am. Coll. Cardiol.* **2011**, *57*, 1314–1322.

(15) Park, S. J.; Kang, S. J.; Virmani, R.; Nakano, M.; Ueda, Y. In-Stent Neoatherosclerosis: A Final Common Pathway of Late Stent Failure. *J. Am. Coll. Cardiol.* **2012**, *59*, 2051–2057.

(16) Versari, D.; Lerman, L. O.; Lerman, A. The Importance of Reendothelialization after Arterial Injury. *Curr. Pharm. Des.* **2007**, *13*, 1811–1824.

(17) Finn, A. V.; Joner, M.; Nakazawa, G.; Kolodgie, F.; Newell, J.; John, M. C.; Gold, H. K.; Virmani, R. Pathological Correlates of Late Drug-Eluting Stent Thrombosis: Strut Coverage as a Marker of Endothelialization. *Circulation* **2007**, *115*, 2435–2441.

(18) Finn, A. V.; Nakazawa, G.; Joner, M.; Kolodgie, F. D.; Mont, E. K.; Gold, H. K.; Virmani, R. Vascular Responses to Drug Eluting Stents: Importance of Delayed Healing. *Arterioscler., Thromb., Vasc. Biol.* **2007**, *27*, 1500–1510.

(19) Nakazawa, G.; Finn, A. V.; Joner, M.; Ladich, E.; Kutys, R.; Mont, E. K.; Gold, H. K.; Burke, A. P.; Kolodgie, F. D.; Virmani, R. Delayed Arterial Healing and Increased Late Stent Thrombosis at Culprit Sites after Drug-Eluting Stent Placement for Acute Myocardial Infarction Patients: An Autopsy Study. *Circulation* **2008**, *118*, 1138–1145.

(20) Santulli, G.; Wronska, A.; Uryu, K.; Diacovo, T. G.; Gao, M.; Marx, S. O.; Kitajewski, J.; Chilton, J. M.; Akat, K. M.; Tuschl, T.; Marks, A. R.; Totary-Jain, H. A Selective MicroRNA-Based Strategy Inhibits Restenosis While Preserving Endothelial Function. *J. Clin. Invest.* **2014**, *124*, 4102–4114.

(21) Haudenschild, C. C.; Schwartz, S. M. Endothelial Regeneration. II. Restitution of Endothelial Continuity. *Lab. Invest.* **1979**, *41*, 407–418.

(22) Stemerman, M. B.; Spaet, T. H.; Pitlick, F.; Cintron, J.; Lejniaks, I.; Tiell, M. L. Intimal Healing. The Pattern of Reendothelialization and Intimal Thickening. *Am. J. Pathol.* **1977**, *87*, 125–142.

(23) Dichek, D. A.; Neville, R. F.; Zwiebel, J. A.; Freeman, S. M.; Leon, M. B.; Anderson, W. F. Seeding of Intravascular Stents with Genetically Engineered Endothelial Cells. *Circulation* **1989**, *80*, 1347–1353.

(24) Kutryk, M. J.; van Dortmont, L. M.; de Crom, R. P.; van der Kamp, A. W.; Verdouw, P. D.; van der Giessen, W. J. Seeding of Intravascular Stents by the Xenotransplantation of Genetically Modified Endothelial Cells. *Semin. Interv. Cardiol.* **1998**, *3*, 217–220.

(25) Scott, N. A.; Candal, F. J.; Robinson, K. A.; Ades, E. W. Seeding of Intracoronary Stents with Immortalized Human Microvascular Endothelial Cells. *Am. Heart J.* **1995**, *129*, 860–866.

(26) Aoki, J.; Serruys, P. W.; van Beusekom, H.; Ong, A. T.; McFadden, E. P.; Sianos, G.; van der Giessen, W. J.; Regar, E.; de Feyter, P. J.; Davis, H. R.; Rowland, S.; Kutryk, M. J. Endothelial Progenitor Cell Capture by Stents Coated with Antibody against CD34: The Healing-Fim (Healthy Endothelial Accelerated Lining Inhibits Neointimal Growth-First in Man) Registry. *J. Am. Coll. Cardiol.* **2005**, *45*, 1574–1579.

(27) Dimmeler, S.; Leri, A. Aging and Disease as Modifiers of Efficacy of Cell Therapy. *Circ. Res.* **2008**, *102*, 1319–1330.

(28) Gulati, R.; Jevremovic, D.; Peterson, T. E.; Witt, T. A.; Kleppe, L. S.; Mueske, C. S.; Lerman, A.; Vile, R. G.; Simari, R. D. Autologous

Culture-Modified Mononuclear Cells Confer Vascular Protection after Arterial Injury. *Circulation* **2003**, *108*, 1520–1526.

(29) Polyak, B.; Fishbein, I.; Chorny, M.; Alferiev, I.; Williams, D.; Yellen, B.; Friedman, G.; Levy, R. J. High Field Gradient Targeting of Magnetic Nanoparticle-Loaded Endothelial Cells to the Surfaces of Steel Stents. *Proc. Natl. Acad. Sci. U. S. A.* **2008**, *105*, 698–703.

(30) Pislaru, S. V.; Harbuzariu, A.; Gulati, R.; Witt, T.; Sandhu, N. P.; Simari, R. D.; Sandhu, G. S. Magnetically Targeted Endothelial Cell Localization in Stented Vessels. *J. Am. Coll. Cardiol.* **2006**, *48*, 1839–1845.

(31) Adamo, R. F.; Fishbein, I.; Zhang, K.; Wen, J.; Levy, R. J.; Alferiev, I. S.; Chorny, M. Magnetically Enhanced Cell Delivery for Accelerating Recovery of the Endothelium in Injured Arteries. *J. Controlled Release* **2016**, *222*, 169–175.

(32) Vosen, S.; Rieck, S.; Heidsieck, A.; Mykhaylyk, O.; Zimmermann, K.; Bloch, W.; Eberbeck, D.; Plank, C.; Gleich, B.; Pfeifer, A.; Fleischmann, B. K.; Wenzel, D. Vascular Repair by Circumferential Cell Therapy Using Magnetic Nanoparticles and Tailored Magnets. *ACS Nano* **2016**, *10*, 369–376.

(33) Riegler, J.; Liew, A.; Hynes, S. O.; Ortega, D.; O'Brien, T.; Day, R. M.; Richards, T.; Sharif, F.; Pankhurst, Q. A.; Lythgoe, M. F. Superparamagnetic Iron Oxide Nanoparticle Targeting of MSCs in Vascular Injury. *Biomaterials* **2013**, *34*, 1987–1994.

(34) Grant, E. G.; Benson, C. B.; Moneta, G. L.; Alexandrov, A. V.; Baker, J. D.; Bluth, E. I.; Carroll, B. A.; Eliasziw, M.; Gocke, J.; Hertzberg, B. S.; Katanick, S.; Needleman, L.; Pellerito, J.; Polak, J. F.; Rholl, K. S.; Wooster, D. L.; Zierler, R. E. Carotid Artery Stenosis: Gray-Scale and Doppler Us Diagnosis-Society of Radiologists in Ultrasound Consensus Conference. *Radiology* **2003**, *229*, 340–346.

(35) Zwiebel, W. J. Spectrum Analysis in Carotid Sonography. *Ultrasound Med. Biol.* **1987**, *13*, 625–636.

(36) Lindner, V.; Reidy, M. A.; Fingerle, J. Regrowth of Arterial Endothelium. Denudation with Minimal Trauma Leads to Complete Endothelial Cell Regrowth. *Lab. Invest.* **1989**, *61*, 556–563.

(37) Clowes, A. W.; Reidy, M. A.; Clowes, M. M. Kinetics of Cellular Proliferation after Arterial Injury. I. Smooth Muscle Growth in the Absence of Endothelium. *Lab. Invest.* **1983**, *49*, 327–333.

(38) Chorny, M.; Fishbein, I.; Tengood, J. E.; Adamo, R. F.; Alferiev, I. S.; Levy, R. J. Site-Specific Gene Delivery to Stented Arteries Using Magnetically Guided Zinc Oleate-Based Nanoparticles Loaded with Adenoviral Vectors. *FASEB J.* **2013**, *27*, 2198–2206.

(39) Chorny, M.; Fishbein, I.; Yellen, B. B.; Alferiev, I. S.; Bakay, M.; Ganta, S.; Adamo, R.; Amiji, M.; Friedman, G.; Levy, R. J. Targeting Stents with Local Delivery of Paclitaxel-Loaded Magnetic Nanoparticles Using Uniform Fields. *Proc. Natl. Acad. Sci. U. S. A.* **2010**, *107*, 8346–8351.

(40) Finn, A. V.; Gold, H. K.; Tang, A.; Weber, D. K.; Wight, T. N.; Clermont, A.; Virmani, R.; Kolodgie, F. D. A Novel Rat Model of Carotid Artery Stenting for the Understanding of Restenosis in Metabolic Diseases. *J. Vasc. Res.* **2002**, *39*, 414–425.

(41) Fishbein, I.; Alferiev, I.; Bakay, M.; Stachelek, S. J.; Sobolewski, P.; Lai, M.; Choi, H.; Chen, I. W.; Levy, R. J. Local Delivery of Gene Vectors from Bare-Metal Stents by Use of a Biodegradable Synthetic Complex Inhibits In-Stent Restenosis in Rat Carotid Arteries. *Circulation* **2008**, *117*, 2096–2103.

(42) Fishbein, I.; Forbes, S. P.; Adamo, R. F.; Chorny, M.; Levy, R. J.; Alferiev, I. S. Vascular Gene Transfer from Metallic Stent Surfaces Using Adenoviral Vectors Tethered through Hydrolyzable Cross-Linkers. *J. Visualized Exp.* **2014**, DOI: 10.3791/51653.

(43) Indolfi, C.; Esposito, G.; Stabile, E.; Cavuto, L.; Pisani, A.; Coppola, C.; Torella, D.; Perrino, C.; Di Lorenzo, E.; Curcio, A.; Palombini, L.; Chiariello, M. A New Rat Model of Small Vessel Stenting. *Basic Res. Cardiol.* **2000**, *95*, 179–185.

(44) Zohra, F. T.; Medved, M.; Lazareva, N.; Polyak, B. Functional Behavior and Gene Expression of Magnetic Nanoparticle-Loaded Primary Endothelial Cells for Targeting Vascular Stents. *Nanomedicine (London, U. K.)* **2015**, *10*, 1391–1406.

(45) Orynbayeva, Z.; Sensenig, R.; Polyak, B. Metabolic and Structural Integrity of Magnetic Nanoparticle-Loaded Primary Endothelial Cells

for Targeted Cell Therapy. *Nanomedicine (London, U. K.)* **2015**, *10*, 1555–1568.

(46) Fischer, U. M.; Harting, M. T.; Jimenez, F.; Monzon-Posadas, W. O.; Xue, H.; Savitz, S. I.; Laine, G. A.; Cox, C. S., Jr. Pulmonary Passage is a Major Obstacle for Intravenous Stem Cell Delivery: The Pulmonary First-Pass Effect. *Stem Cells Dev.* **2009**, *18*, 683–692.

(47) Schrepfer, S.; Deuse, T.; Reichenspurner, H.; Fischbein, M. P.; Robbins, R. C.; Pelletier, M. P. Stem Cell Transplantation: The Lung Barrier. *Transplant. Proc.* **2007**, *39*, 573–576.

(48) Nugent, H. M.; Ng, Y. S.; White, D.; Groothuis, A.; Kanner, G.; Edelman, E. R. Ultrasound-Guided Percutaneous Delivery of Tissue-Engineered Endothelial Cells to the Adventitia of Stented Arteries Controls the Response to Vascular Injury in a Porcine Model. *J. Vasc. Surg.* **2012**, *56*, 1078–1088.

(49) Timmins, L. H.; Miller, M. W.; Clubb, F. J., Jr.; Moore, J. E., Jr. Increased Artery Wall Stress Post-Stenting Leads to Greater Intimal Thickening. *Lab. Invest.* **2011**, *91*, 955–967.

(50) Hoffmann, R.; Mintz, G. S.; Dussallant, G. R.; Popma, J. J.; Pichard, A. D.; Satler, L. F.; Kent, K. M.; Griffin, J.; Leon, M. B. Patterns and Mechanisms of In-Stent Restenosis. A Serial Intravascular Ultrasound Study. *Circulation* **1996**, *94*, 1247–1254.

(51) Berry, J. L.; Manoach, E.; Mekkaoui, C.; Rolland, P. H.; Moore, J. E., Jr.; Rachev, A. Hemodynamics and Wall Mechanics of a Compliance Matching Stent: *In Vitro* and *In Vivo* Analysis. *J. Vasc. Interv. Radiol.* **2002**, *13*, 97–105.

(52) Adams, C. F.; Rai, A.; Sneddon, G.; Yiu, H. H.; Polyak, B.; Chari, D. M. Increasing Magnetite Contents of Polymeric Magnetic Particles Dramatically Improves Labeling of Neural Stem Cell Transplant Populations. *Nanomedicine* **2015**, *11*, 19–29.

(53) MacDonald, C.; Barbee, K.; Polyak, B. Force Dependent Internalization of Magnetic Nanoparticles Results in Highly Loaded Endothelial Cells for Use as Potential Therapy Delivery Vectors. *Pharm. Res.* **2012**, *29*, 1270–1281.

(54) Tengood, J. E.; Alferiev, I. S.; Zhang, K.; Fishbein, I.; Levy, R. J.; Chorny, M. Real-Time Analysis of Composite Magnetic Nanoparticle Disassembly in Vascular Cells and Biomimetic Media. *Proc. Natl. Acad. Sci. U. S. A.* **2014**, *111*, 4245–4250.

(55) MacDonald, C.; Friedman, G.; Alamia, J.; Barbee, K.; Polyak, B. Time-Variied Magnetic Field Enhances Transport of Magnetic Nanoparticles in Viscous Gel. *Nanomedicine (London, U. K.)* **2010**, *5*, 65–76.

(56) Cohen, G.; Lecht, S.; Arien-Zakay, H.; Ettinger, K.; Amsalem, O.; Oron-Herman, M.; Yavin, E.; Prus, D.; Benita, S.; Nissan, A.; Lazarovici, P. Bio-Imaging of Colorectal Cancer Models Using Near Infrared Labeled Epidermal Growth Factor. *PLoS One* **2012**, *7*, e48803.

(57) Schwartz, R. S.; Huber, K. C.; Murphy, J. G.; Edwards, W. D.; Camrud, A. R.; Vlietstra, R. E.; Holmes, D. R. Restenosis and the Proportional Neointimal Response to Coronary Artery Injury: Results in a Porcine Model. *J. Am. Coll. Cardiol.* **1992**, *19*, 267–274.

(58) Granta Design Limited. www.grantadesign.com (accessed April 12, 2016).

(59) Blandford, R. K.; Morton, D. K.; Snow, S. D.; Rahl, T. E. Tensile Stress-Strain Results for 304L and 316L Stainless Steel Plate at Temperature. *2007 ASME Pressure Vessels and Piping Division Conference* **2007**, 617. <https://inldigitallibrary.inl.gov/sti/3772045.pdf>.

(60) Chen, S. I.; Tsai, C. H.; Liu, J. S.; Kan, H. C.; Yao, C. M.; Lee, L. C.; Shih, R. J.; Shen, C. Y., The Biomechanical Analysis of the Coil Stent and Mesh Stent Expansion in the Angioplasty. In *13th International Conference on Biomedical Engineering: ICBME 2008 3–6 December 2008 Singapore*, Lim, C. T., Goh, J. C. H., Eds.; Springer Berlin Heidelberg: Berlin, Heidelberg, 2009; pp 1592–1594.